Investigation of Phase Morphology, Thermal Behavior, and Impact Properties of Polyamide-1010/Polystyrene Blends Compatibilized by Lightly Sulfonated Polystyrene Ionomers

HAIPENG LI, ZHUOMEI LI

Institute of Polymer Science, Zhongshan University, Guangzhou, People's Republic of China, 510275

Received 26 December 1996; accepted 6 June 1997

ABSTRACT: The phase morphology, thermal behavior, and impact properties of polyamide-1010 (PA)/polystyrene (PS) blends compatibilized by sulfonated polystyrene (HSPS) and their zinc salts (ZnSPS) were investigated, using a dynamic mechanical analyzer (DMA), a scanning electron microscope (SEM), a differential scanning calorimetry (DSC), and a pendulum impact tester. It was found that the addition of the ionomer had an improved effect on the phase morphology of the resulting blends, where the HSPS was a more effective compatibilizer than was the ZnSPS due to its low melt viscosity and less self-agglomeration in the PA matrix. DSC results showed that with increasing the ionomer content the amount of the less perfect crystals of PA increased in these blends and, hence, led to a small increase in the crystallinity of the PA phase. The crystallization rate of the PA in the resulting blends was accelerated slightly by the ZnSPS but was decreased by the HSPS, which was probably due to the nucleation effect of ZnSPS for PA but no nucleation of HSPS. The best improvement in the notched impact strength of the blends was achieved with the content of the ionomer up to 20 wt % based on the amount of PS. © 1998 John Wiley & Sons, Inc. J Appl Polym Sci **67:** 61–69, 1998

INTRODUCTION

It is well known that in 1984 a new concept (relative to the traditional concept of rubber toughening) of rigid organic filler toughening was put forth by Kurauchi and Ohta[1] through studies on plastic blends composed of a ductile matrix and dispersed brittle particles. The mechanism of this rigid organic filler toughening is that the impact energy is absorbed by a large plastic deformation of the brittle particles dispersed in a ductile matrix, which is known as "cold drawing."

Among the various combinations of brittle/ductile polymers, the polyamide/polystyrene system showed very poor mechanical properties,[2] which was primarily attributed to the poor miscibility and little interfacial adhesion between the two phases. Approaches to the improvement in miscibility of polyamide and polystyrene have therefore focused on systems where polyamide is blended with a styrene copolymer, such as the styrene–maleic anhydride copolymer[3] or ABS.[4–6] Since the good adhesion between the brittle particle and the ductile matrix may be essential for proper stress transfer to induce cold drawing,[7] it is expected that the addition of a third component (such as an ionomer) into the polyamide/polystyrene binary blend would change the morphology and thus affect significantly the mechanical properties (such as impact strength) of the final blends.

Correspondence to: Z. Li.

Contract grant sponsors: Foundation of Specialties Opened to Doctorate Studies, China; Ma Canan Educational Foundation.

Journal of Applied Polymer Science, Vol. 67, 61–69 (1998)
 CCC 0021-8995/98/010061-09

The brittle/ductile combination selected in this study was polystyrene/polyamide-1010. Sulfonated polystyrene and their zinc salts are expected to be compatibilizers for the polyamide-1010/polystyrene binary system, since the backbone of sulfonated polystyrene is miscible with polystyrene and a strong interaction exists between amide groups and either sulfonic acid or zinc sulfonate groups.[8–10]

We focused our investigation on the effect of an ionomer on the miscibility, morphology, thermal behavior, and impact strength of the resulting blend systems and the importance of interfacial adhesion for toughening in the brittle/ductile binary system.

EXPERIMENTAL

Materials

Atactic polystyrene (PS) with M_n = 79,300 was obtained from the Hannam Chemical Corp., South Korea. Sulfonated polystyrene (HSPS) was prepared by sulfonating polystyrene in 1,2-dichloroethane at 50°C using acetyl sulfate as the sulfonating agent.[11] The sulfonation level in this work was 3.6 mol % by titration of the polymer in a toluene/methanol (90 : 10 v/v) solution with sodium hydroxide in methanol. Zinc salts of sulfonated polystyrene (ZnSPS) were prepared by neutralizing the sulfonated polystyrene with a 10% excess of zinc acetate. Polyamide-1010 (PA) was supplied by the Shanghai Celluloid Factory, a II type product with a melting point of 200°C and relative viscosity of 1.9.

Melt Blending

Melt blends were prepared in an XSS-300 torque rheometer by molten mixing for 8 min at 230°C and 33 rpm under 5 kg.

Dynamic Mechanical Analysis (DMA)

Dynamic mechanical properties of blends were determined using a Rheovibron DDV-II-EA dynamic mechanical analyzer at a heating rate of 3°C/min and a frequency of 110 Hz. The sample size was approximately 20 × 3 × 0.1 mm.

Scanning Electron Microscopy (SEM)

Morphological observation was performed on a Hitachi S-520 SEM. The samples for SEM were obtained from compression-molded sheets fractured in liquid nitrogen.

Thermal Analysis

Thermal analysis was performed on a Perkin-Elmer DSC 7 apparatus. The samples were exposed to the following conditions: The specimens (3–5 mg), encapsulated in aluminum pans, were rapidly heated to 230°C, held 5 min at this temperature to cancel their thermal history, cooled to 100°C at a scanning rate of 10°C/min, and eventually heated again to 230°C at the same rate. All the measurements were performed under a nitrogen atmosphere. The recorded temperatures were calibrated using Indium as standards.

Notched Charpy Impact Strength Testing

Samples for notched charpy strength testing were prepared by mold pressing at 230°C under 15 MPa for 5 min and then cooled slowly at ambient temperature. A sample size of 55 ± 1 × 6 ± 0.2 × 4 ± 0.2 mm^3 with a notch depth of the one-third of the thickness and a notch width of 0.8 mm was taken for charpy impact strength testing on a pendulum impact tester with a gap span of 40 mm. Before measurement, the samples were equilibrated under ambient conditions (22°C and 58% RH) for at least 24 h. The reported data are the average values of five to seven measurements.

RESULTS AND DISCUSSION

Dynamic Mechanical Analysis (DMA)

DMA was used to determine the miscibility of the blends by investigating the variation of the glass transition temperature (T_g) of the blend components. Tan δ was plotted as a function of temperature for the starting materials and their blends in Figure 1. The temperature ranges of all tan δ peaks and the maximum values of the PA tan δ peaks are summarized in Table I.

For the PS10 blend, two distinct tan δ peaks were discernible. The broad one was due to the T_g of PA (PA-T_g), while the sharp peak at 119°C was due to the T_g of PS (PS-T_g). In contrast to pure PA, the T_g region of PA in the PS10 blend, with a slightly higher onset temperature, was broader, which suggests that a small fraction of the PS was miscible with the amorphous phase of

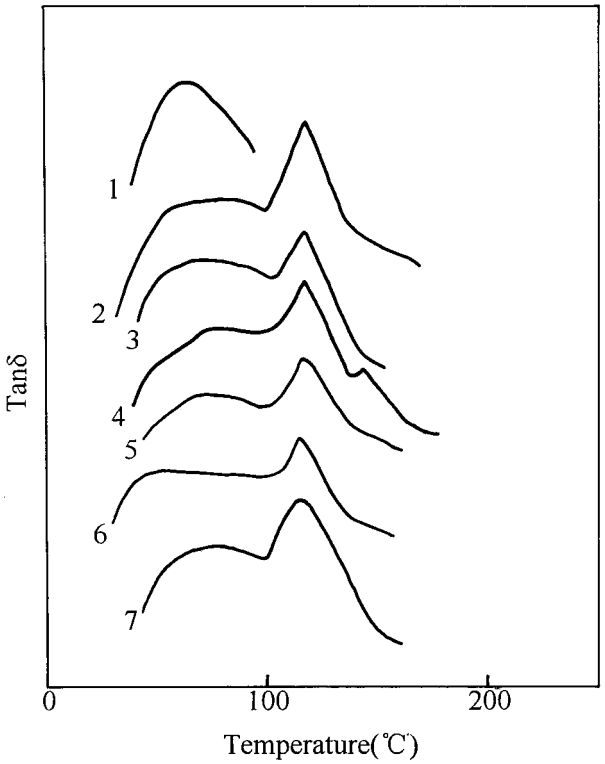

Figure 1 Tan δ vs. temperature for (1) PA, (2) PS10, (3) Zn2, (4) Zn4, (5) H1, (6) H2, and (7) H4.

PA although there was little interaction between them.

The addition of ZnSPS to the PS10 blend caused the PA-T_g to shift toward the PS-T_g and the shift became more evident as the addition of ZnSPS increased, whereas no shift was observed for PS-T_g. This indicated that by using ZnSPS as a compatibilizer the miscibility between PA and PS phases was improved as the motions of the PA segments in the PA-rich phase were hindered by the interpenetration of the PS segments into the PA phase. This improvement in miscibility was more remarkable as the HSPS was used instead of the ZnSPS. For sample H1, it could be seen that the onset temperature of the PA-T_g region shifted toward the PS-T_g, and, meanwhile, the PS-T_g shifted inward slightly, showing that the simultaneous interpenetration occurred between PA and PS by adding a very small amount of the HSPS. Furthermore, this shift toward each other developed as observed from sample H2 in that the T_g region of PA became a broad "platform" (which implied a broad interface was formed between the two phases) and the PS-T_g shifted to a temperature lower than that of sample H1. The formation of the broad "platform" for the PA-T_g region could be explained in terms of the rather complex relaxation of PA segments in the broad interphase. On the one hand, the relaxation of some PA segments in the broad interphase was hindered by PS segments, which led to the higher T_g temperature for these PA segments. But, on the other hand, due to the disruption of the strong intermolecular interaction (hydrogen bonding) among PA segments replaced by the interaction between amide groups and sulfonic acid groups, some PA was "released" and became the "free" segments which showed a lower T_g. Hence, it was not difficult to understand that the opposite trends for the shift of the PA-T_g should be responsible to the broadening of the PA-T_g region for sample H2. It can be inferred that the relaxation of PS may be affected considerably by the increasing number of the "free" PA segments with increasing HSPS conent. This was in accord with the observation for sample H4 where the tan δ peak of PS became somewhat broad, showing the complexity of PS relaxation with the existence of the increasing "free" PA segments.

It was noticed that for sample Zn4 an ionomer tan δ "peak" (143.8°C) appeared as a shoulder on

Table I DMA Results of Starting Materials and Blends

Blend Code	Blend Composition (Weight Ratio)	DMA tan δ Peak Temperature (°C)	PA tan δ Maximum
PA	Polyamide	64–71.4	0.109
PS	Polystyrene	119.4	—
PS10	90/10 PA/PS	65.3–83.4, 119.4	0.088
Zn2	90/10/2 PA/PS/ZnSPS	68.6–80.6, 119.6	0.095
Zn4	90/10/4 PA/PS/ZnSPS	74.9–86.8, 119.8, 143.8	0.080
H1	90/10/1 PA/PS/HSPS	69.9–76.0, 117.9	0.113
H2	90/10/2 PA/PS/HSPS	47.3–91.9, 116.0	0.114
H4	90/10/4 PA/PS/HSPS	69.9–75.9, 114.8–117.8	0.099

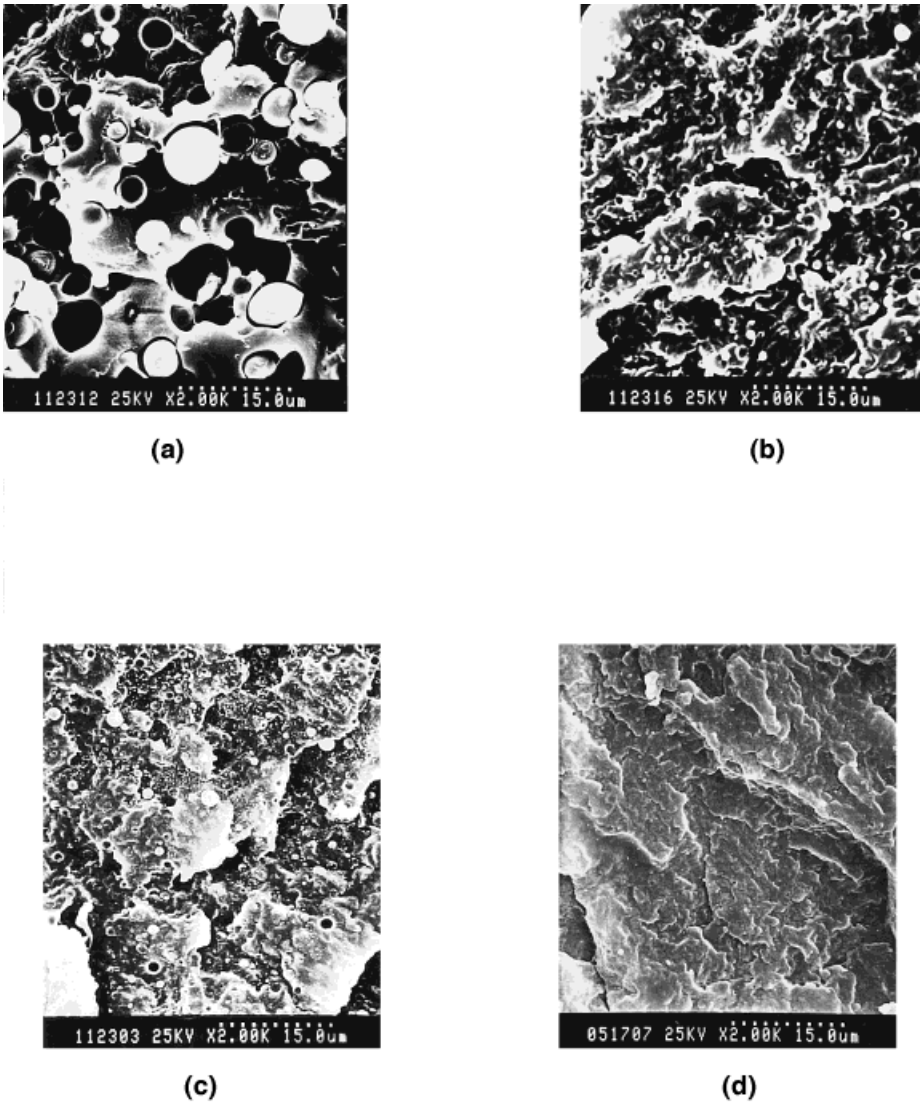

Figure 2 Scanning electron micrographs of (a) PS10, (b) Zn2, (c) Zn4, and (d) H2 (the sample codes are shown in Table I).

the tan δ peak of PS, suggesting that an ionomer phase, which was immiscible with either PA or PS, existed in this sample. But for H4, no such ionomer phase was detected by DMA at the same condition. Based on the point that the neutralization of sulfonated polystyrene with metal counterions dramatically increased its melt viscosity due to the stronger ionic aggregation, one may expect that the lower melt viscosity of HSPS than of ZnSPS facilitates the dispersion of HSPS in the matrix by reducing the ionomer agglomeration and by acting as compatibilizers much more effectively than did ZnSPS.

The effect of the ionomer content on the maximum of PA loss tangent peak was analogous for either the ZnSPS or the HSPS compatibilized blends. Compared to the PS10 blend, the PA tan δ maximum increased first with the addition of the ionomer of no more than 20 wt % based on the PS phase, showing the increasing internal friction in the motions of the PA segments caused by the interaction between the ionomer and the PA. As indicated in the differential scanning calorimetry (DSC) analysis that the crystallinity of the PA phase increased with increasing ionomer content, this result could be the cause of the decrease in the maximum of PA tan δ peak with the reduction in the volume fraction of PA amorphous phase as the ionomer content was beyond 20 wt % based on the amount of PS.

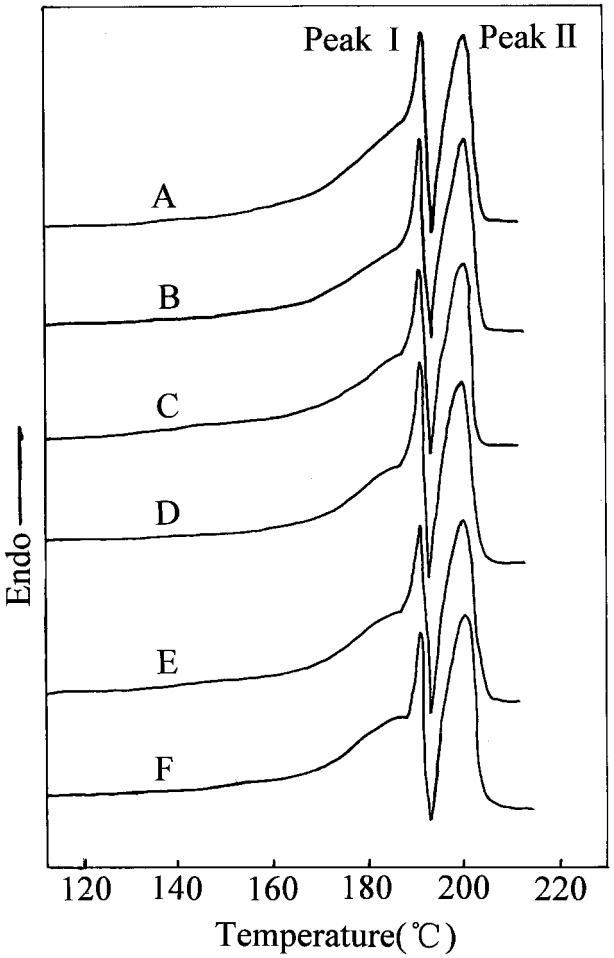

Figure 3 DSC fusion thermograms for PA, PA/PS, and PA/PS/ZnSPS blends: (A) PA; (B) PS10; (C) Zn1; (D) Zn2; (E) Zn4; (F) Zn6.

Morphology

The SEM micrographs of the cryogenically fractured molded sheets of PS10 and its compatibilized blends are shown in Figure 2. The morphology of the PS10 blend showed the typical morphology of an incompatible blend where the PS domain had a well-defined spherical shape with a diameter between ca. 2 and 10 μm. The domain surface and the surface of the holes left by the PS spheres appeared very smooth, suggesting a poor adhesion between the two phases.

Great differences were clearly observed between the morphology of the sample of PS10 and Zn2. For the Zn2 sample, the average size of the PS domains decreased greatly with the diameter ranging between about 1.2 and 0.6 μm and the distribution of the size was more homogeneous. This result showed that an improved miscibility between the two phases was present in this blend. However, heterodispersement of the particle size was observed when the additive amount of ZnSPS increased. As for the Zn4 sample, a large amount of fine granules appeared, and, meanwhile, a small amount of larger particles (size about 1.5–2.5 μm) was observed also. With reference to the DMA results, it was reasonable to infer that the fine granules were the PS component, while the larger particles might be ZnSPS ionomer particles agglomerated in the PA matrix due to their great melt viscosity during blending.

By replacing ZnSPS with HSPS as the compatibilizer, it was observed from the morphology of H2 that almost no PS domain was detected by the SEM at this enlargement. This was in agreement with the DMA results that for the PA/PS blend HSPS was the more effective compatibilizer than

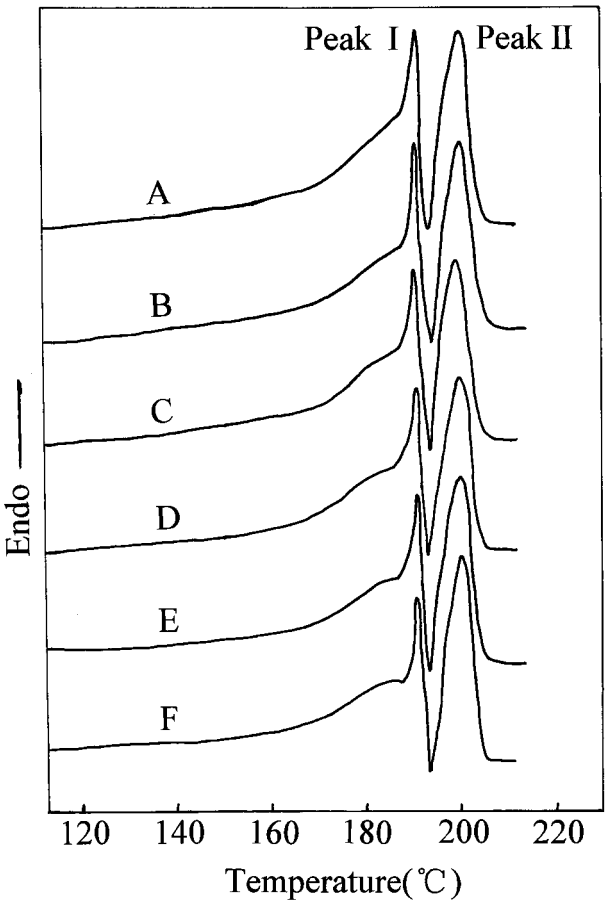

Figure 4 DSC fusion thermograms for PA, PA/PS and PA/PS/HSPS blends: (A) PA; (B) PS10; (C) H1; (D) H2; (E) H4; (F) H6.

Table II Thermal Analysis of PA1010 and Its Blends by DSC

Blend Code	Composition (Weight Ratio)	T_m[a] (°C)		T_c[d] (°C)	ΔH_f[c] (J/g)	ΔH_c[d] (J/g)	Tonset-T_c (°C)
		T_{m_1}	T_{m_2}				
PA	Polyamide	191.53	200.33	176.75	83.58	60.78	5.44
PS10	90/10 PA/PS	191.47	200.35	176.11	82.53	60.51	5.59
Zn1	90/10/1 PA/PS/ZnSPS	190.93	200.25	176.44	84.76	60.83	5.20
Zn2	90/10/2 PA/PS/ZnSPS	190.87	199.76	176.58	82.00	60.21	5.13
Zn4	90/10/4 PA/PS/ZnSPS	191.02	200.00	176.13	84.30	63.37	5.37
Zn6	90/10/6 PA/PS/ZnSPS	191.02	200.50	176.53	88.27	67.02	5.17
H1	90/10/1 PA/PS/HSPS	190.81	199.90	174.81	82.23	61.38	5.98
H2	90/10/2 PA/PS/HSPS	191.27	200.16	174.71	82.75	62.64	6.38
H4	90/10/4 PA/PS/HSPS	191.09	200.15	174.89	84.36	64.69	6.40
H6	90/10/6 PA/PS/HSPS	190.97	200.65	175.25	88.18	67.84	6.64

[a] T_m = Melting peak temperature.
[b] T_c = Crystallized peak temperature.
[c] ΔH_f = heat of fusion.
[d] ΔH_c = heat of crystallization.

was the ZnSPS by forming a broad interphase between the two phases.

Thermal Analysis

To evaluate the thermal behavior of PA in the blends prepared, fusion and crystalization thermograms were obtained by DSC. The DSC fusion thermograms of the PA and the blends are shown in Figures 3 and 4 and the results of the measurements are summarized in Table II.

In the fusion thermogram of PA, which was nonisothermally crystallized in the present study, two distinct melting peaks were detected. Based on the research on PA-1010 recrystallization and the melting process during thermal scanning made by Fu et al.[12,13] and on the research in the properties of PA-1010 spherulites made by Zhu,[14–16] and also taking into the consideration that the heating rate (10°C/min) in the present measurement was relatively low, the multiple melting behavior in the fusion thermogram of the PA in this work could be explained as follows: The two peaks (I and II) with clear peak temperatures would be, respectively, attributed to the melting behavior of the different types of the nonringed spherulites, in which the one at lower temperature (peak I) was due to the melting of the mixed nonringed spherulite, while the other one (peak II), to the melting of the positive nonringed spherulite recrystallized during the thermal scanning. In addition, a flat endothermal "peak" was also observed as the shoulder of peak I, which was due to the melting of the less perfect crystals growing from the melt during the nonisothermal crystallization.

The sample of PS10 showed a melting endotherm consisting of two distinguishable peaks very similar to PA. By adding the ionomer as the compatibilizer into the PS10 blend, a similar effect was observed for either the ZnSPS or the HSPS compatibilized blends. Although the temperatures for peak I and peak II only shifted slightly, the height of peak I decreased gradually (except for the sample of Zn2) relative to peak II as the ionomer increased and was somewhat more evident for HSPS than for ZnSPS. This probably resulted from the observation mentioned above that the growth of the mixed nonringed spherulite was hindered by the added ionomer and, probably, the transformation of the mixed nonringed spherulite to the more thermally stable positive nonringed spherulite occurred during the thermal scanning of the sample.

Another similar effect which should not be ignored for either the ZnSPS or the HSPS compatibilized blends was that with increasing content of the ionomer the flat endothermal "peak" became somewhat higher and looked more like a peak bundle with a slightly distinguishable peak temperature. This fact may imply that as the addition of the ionomer increased the amount of the less perfect crystals of PA also increased to a certain extent, large enough to show their own melting points.

The crystallization behavior of the PA in the

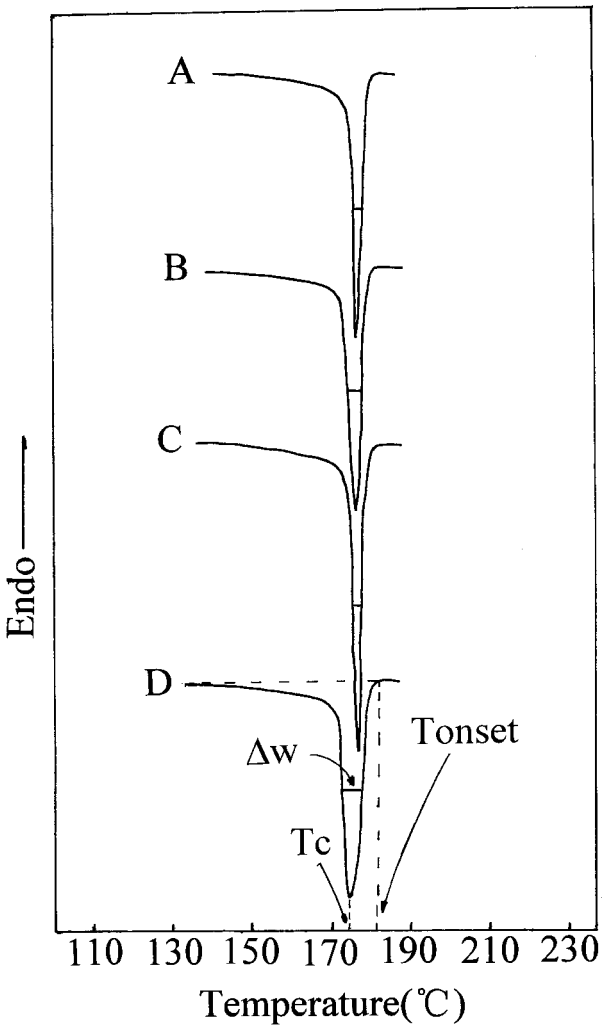

Figure 5 DSC crystallization thermograms for PA, PA/PS, and PA/PS/ionomer blends: (A) PA; (B) PS10; (C) Zn2; (D) H2.

blends was studied by the DSC crystallization thermograms recorded during the cooling of the sample from the melt. The results are discussed in terms of the following quantities shown in Figure 5[17,18]: (1) T_c—the higher the T_c, the easier the PA crystallized; (2) the value of the Tonset-T_c—the smaller the value of the Tonset-T_c, the faster the PA crystallization rate; and (3) the half-width of the PA crystallization peak (Δw), as a measure of the distribution of crystallite size.

As shown in Table II, the values of the Tonset-T_c of the ZnSPS compatibilized blends were somewhat smaller than that of PS10 sample but their T_c's were nearly unchanged. For the HSPS compatibilized blends, the T_c's were lower by no more than 2°C compared to the PS10 sample and, correspondingly, an increase in the values of the Tonset-T_c was also observed. Thus, the crystallization rate of PA in the blends was accelerated slightly by the ZnSPS but decreased by the HSPS. Taking into the consideration that the rate of nucleation is the critical step in determining the crystallization rate, it could be assumed that the ZnSPS played the role of the crystal nucleus when PA in the blends were crystallized from the melt.

As illustrated in Figure 5, the ZnSPS compatibilized blend had a smaller half-width of the PA crystallization peak than that of the PS10 sample, while for the blend compatibilized by the HSPS, the peak width was larger than that of the PS10 sample. This result indicated that the size distribution of the PA crystallites in the blends was reduced by the addition of the ZnSPS but increased with the HSPS, which may be attributed to the more effective nucleation of the ZnSPS in the blends than that of the HSPS.

Table II shows that as the addition of the ionomer increased either the heat of fusion or the heat of crystallization of the PA matrix increased, showing a small increase in the crystallinity of the PA phase which was probably related to the increasing formation of the less perfect crystals.

Notched Impact Strength

It is known that the impact strength of PA1010 is sensitive to a notch and has a low energy of crack propagation, resulting in a lower notched impact strength compared to that of PA6, PA66, etc. So, in this article, we focused the mechanical testing of the samples on the notched impact strength measurement to investigate the effect of the improved compatibility made by the ionomer on the notched toughness of the final blends. The relationship between the notched impact strength of the PA/PS binary blends and the weight fraction of the PS is presented in Figure 6. The notched impact strength decreased rapidly with increasing PS content. This result, as expected, was due to the poor miscibility and small interfacial adhesion between the two phases.

Figure 7 presents the variation of the notched impact strength of the PA/PS/ionomer ternary blends against the content of the ionomer (where the PA/PS was fixed at 90/10 wt/wt). The curves show that the introduction of 20 wt % of the ionomer (based on the PS content) resulted in the maximum improvement in the notched impact strength, where the improvement made by the addition of the HSPS was better than that of the ZnSPS. With further increase in the ionomer

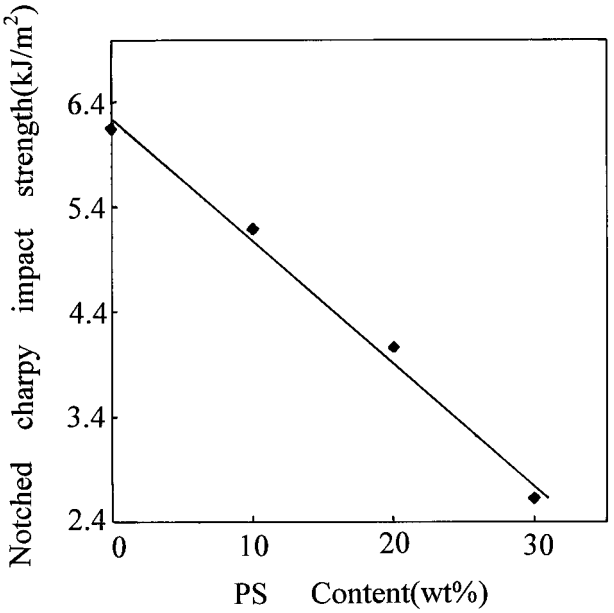

Figure 6 Variation of notched impact strength of PA/PS blends with weight fraction of PS.

level, the notched impact strength sharply decreased. In fact, when the addition of the ionomer was beyond 20 wt % based on the PS content, a large amount of the PS domains were observed on the impact-fracture surface by SEM, which was probably related to the existence of the "loose interface" between the two phases by introducing

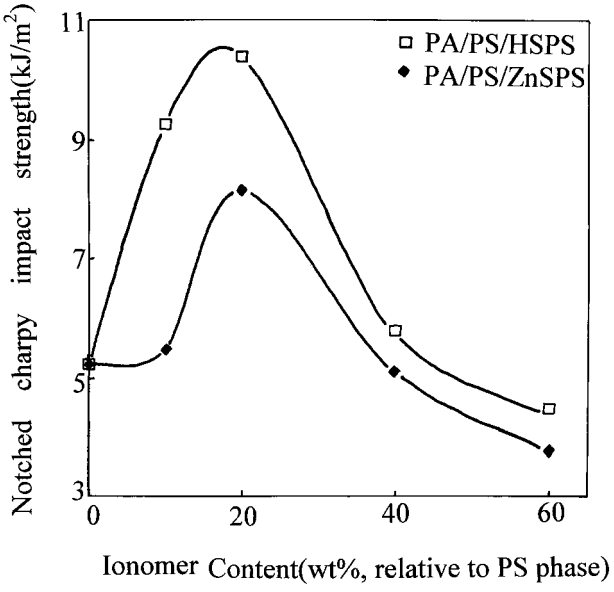

Figure 7 Variation of notched impact strength of PA/PS/ionomer blends with weight fraction of ionomer (relative to the amount of PS).

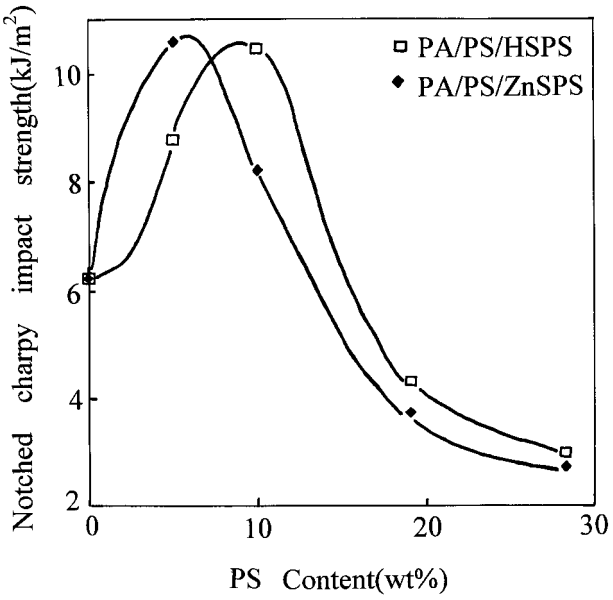

Figure 8 Variation of notched impact strength of PA/PS/ionomer blends with weight fraction of PS (the ionomer was fixed at 20 wt % relative to the amount of PS).

the excess ionomer. In addition, for the ZnSPS compatibilized blends, the excess ZnSPS ionomer could remain in an agglomerated form in the PA matrix due to its high melt viscosity, providing the stress concentration points in the testing.

When the addition of the ionomer was kept unchanged at 20 wt % relative to the amount of PS, the dependence of the notched impact strength of the PA/PS/ionomer blends on the weight fraction of PS was as presented in Figure 8. For either the ZnSPS or the HSPS compatibilized blends, the improved effect on the notched toughness was achieved only when the amount of PS was no more than 10 wt %. This result seemed to be in accord with the general trend that occurred in the system toughened by a rigid organic filler in that the amount of rigid organic filler should not be too large for improvement in the impact strength.[2]

This work was supported by the Foundation of Specialties Opened to Doctorate Studies, People's Republic of China, and in part by the Ma Canan Educational Foundation.

REFERENCES

1. T. Kurauchi and T. Ohta, *J. Mater. Sci.,* **19,** 1669 (1984).

2. K. Koo, T. Inoue, and K. Miyasaka, *Polym. Eng. Sci.,* **25,** 741 (1985).
3. R. Vankan, P. Degée, R. Jérôme, and P. Teyssié, *Polym. Bull.,* **33,** 221 (1994).
4. A. R. Padwa and R. E. Lavengood, *Polym. Prepr.,* **33,** 600 (1992).
5. H. J. Radusch, M. Stolp, and A. K. Bledzki, *Kunststoffe,* **83,** 557 (1993).
6. B. Majumdar, H. Keskkula, and D. R. Paul, *Polymer,* **35,** 5453 (1994).
7. J. Angola, Y. Fujita, T. Sakai, and T. Inoue, *J. Polym. Sci. Part B Polym. Phys.,* **26,** 807 (1988).
8. A. Molnár and A. Eisenberg, *Polym. Eng. Sci.,* **32,** 1665 (1992).
9. X. Lu and R. A. Weiss, *Macromolecules,* **25,** 6185 (1992).
10. T. K. Kwei, Y. K. Dai, X. Lu, and R. A. Weiss, *Macromolecules,* **26,** 6583 (1993).
11. S. Makowski, R. D. Lundberg, and G. H. Singhai, U.S. Pat. 3,870,841 (1975).
12. Y. Wei and S. Fu, Syn. Fiber Ind. (in Chinese), **13,** 20 (1990).
13. S. Fu and Y. Wei, *J. Thermal Anal.,* **36,** 999 (1990).
14. C. Zhu, J. Wang, G. Yang, Z. Mo, L. Li, and B. Yang, *Acta Polym. Sin.* (in Chinese), **4,** 165 (1993).
15. C. Zhu, X. Li, H. Li, and G. Yang, *Acta Polym. Sin.* (in Chinese), **4,** 449 (1992).
16. C. Zhu, J. Wang, X. Li, S. Pu, and G. Yang, Acta Polym. Sin. (in Chinese), **6,** 728 (1991).
17. A. K. Gupta, V. B. Gupta, R. H. Peters, W. G. Harland, and J. P. Berry, *J. Appl. Polym. Sci.,* **27,** 4669 (1982).
18. A. K. Gupta and S. N. Purwar, *J. Appl. Polym. Sci.,* **29,** 1595 (1984).